



Article

The Effect of Acceptor Structure on Emission Color Tuning in Organic Semiconductors with D- π -A- π -D Structures

Przemyslaw Ledwon ^{1,*}, Gabriela Wiosna-Salyga ^{2,*}, Marian Chapran ² and Radoslaw Motyka ¹

¹ Faculty of Chemistry, Silesian University of Technology, Strzody 9, 44-100 Gliwice, Poland

² Department of Molecular Physics, Lodz University of Technology, Zeromskiego 116, 90-924 Lodz, Poland

* Correspondence: przemyslaw.ledwon@polsl.pl (P.L.); gabriela.wiosna-salyga@p.lodz.pl (G.W.-S.); Tel.: +48-32-237-1305 (P.L.); +48 42-631-3205 (G.W.-S.)

Received: 18 July 2019; Accepted: 13 August 2019; Published: 17 August 2019



Abstract: A series of novel donor-acceptor D- π -A- π -D compounds were synthesized and characterized in order to determine the influence of different acceptor units on their properties. The introduction of acceptor moieties had a direct impact on the HOMO and LUMO energy levels. Fluorescence spectra of compounds can be changed by the choice of an appropriate acceptor and were shifted from the green to the near-infrared part of spectra. Due to observed concentration induced emission quenching, the green exciplex type host was used to evaluate the potential of synthesized molecules as emitters in organic light emitting diodes (OLEDs).

Keywords: fluorescence; electron-acceptor units; charge transfer; near-infrared emission; organic light emitting diode (OLED)

1. Introduction

Donor-acceptor compounds are an important group of π -conjugated organic materials. One of the main factors affecting the properties of such fluoresecent compounds is their structure, which includes a donor, an acceptor, and a linker between the two. Some research has focused on the effects of different acceptor units on photophysical properties [1–4], but most studies have mainly focused on photovoltaic applications [5–7].

In recent years, there has been a growing interest in near-infrared (NIR) to deep-red emitters [8], because of their possible applications in telecommunication and night vision technologies. There is also an increasing demand for NIR emitters in sensing, in areas such as medicine [9], optical communication, lasers, and the automotive industry. This means that the market for these devices in the near future may be one of the most rapidly developed areas of research. In this respect, a study focusing on emission tuning to achieve deep-red and infrared emission is important. For this reason, the development of new emitters with an entire palette of emission colors is highly justified.

Emitters for organic light emitting diodes (OLEDs) can be divided into inorganic semiconductors, metal complexes, and organic compounds [10,11], and there is growing interest in completely OLEDs. Currently, most commercially-available OLEDs are mainly based on Ir or Pt emitters because of their high efficiency and working stability [12–14]. In such devices, the emission layer consists of the host organic material and guest phosphorescence dopant. The main drawback of such devices is the use of precious metals, which results in irreversible damage to the environment. One of the most promising solutions is the use of fully organic fluorescent emitters which exhibit thermally activated delayed fluorescence (TADF) [15–17]. In the typical fluorescence-based devices a neat film of the emitter or the

host-guest system can be used as an emission layer [18]. In addition, a common fluorescent molecule combined with a TADF emitter can be used in hyperfluorescent OLEDs [19]. In such devices, a TADF emitter acts as a sensitizer that harvests excitons and transfers them to a fluorescent emitter by Förster energy transfer [20]. This could be an important strategy that will enable the fabrication of efficient and stable fully-organic OLEDs.

The latest reports indicate that purely fluorescent organic materials can be also efficient NIR emitters [21–25]. One of the most promising strategies used to obtain organic molecules with emission in the red and infrared range is the connection of a strong electron-acceptor (A) unit with a strong electron-donor (D) unit to form polymer or oligomer with structure D–A, D–A–D or A–D–A [26]. The structure can also be modified by adding a π -conjugated bridge (π) which can increase the effective conjugation length. The choice of the appropriate D, A, and π units is crucial to control over the material functionality. Carbazole is one of the most frequently used donor units in many D–A type of dyes, owing to its advantages, such as high luminescent efficiency and broad ability to modify its structure [27]; so far different electron-accepting moieties and their derivatives, including benzoselenadiazole [28], benzothiadiazole [29], quinoxaline [30], and thienopyrroledione [31] were reported as acceptor units with low LUMO levels. However, there are only a limited number of reports that analyze the impact of different types of strong acceptor units on luminescence properties [32].

In most cases, organic emitters are implemented in multilayer OLED structures fabricated by vacuum deposition, but this approach increases the production costs and restricts the implementation of NIR emitters [33–35]. An alternative to this is the fabrication of OLEDs by solution-based techniques, such as inkjet printing, screen printing, slot die coating, and spin coating. These methods reduce the production costs and can be used to produce large and flexible organic devices. It should be emphasized that to realize this, NIR emitters should be suitable for solution processing techniques. The corresponding approach can be used with donor–acceptor compounds with controlled energy band gaps and responsive emission.

Herein, we report the design, synthesis, and characterization of solution-processable organic semiconductors with D– π –A– π –D structures (Figure 1): 1,3-bis(5-((E)-2-(9-(2-ethylhexyl)-9H-carbazol-3-yl)vinyl)thiophen-2-yl)-5-octyl-4H-thieno[3,4-c]pyrrole-4,6(5H)-dione (**C1**), 5,8-bis(5-((E)-2-(9-(2-ethylhexyl)-9H-carbazol-3-yl)vinyl)thiophen-2-yl)quinoxaline (**C2**), 4,7-bis(5-((E)-2-(9-(2-ethylhexyl)-9H-carbazol-3-yl)vinyl)thiophen-2-yl)-5,6-difluorobenzo[c][1,2,5]thiadiazole (**C3**), 4,7-bis(5-((E)-2-(9-(2-ethylhexyl)-9H-carbazol-3-yl)vinyl)thiophen-2-yl)benzo[c][1,2,5]selenadiazole (**C4**), and 5,5'-bis((E)-2-(9-(2-ethylhexyl)-9H-carbazol-3-yl)vinyl)-2,2'-bithiophene (**C5**). A new series of model molecules was designed and developed to examine the possibility of shifting emissions from the visible to the near-infrared region using common building blocks. Structures containing thiophene, vinyl, and carbazole units were chosen to ensure extensive π -conjugation as a result of the planarization of the vinyl linker, and ethylhexyl groups were used to ensure sufficient solubility of the final compounds. Different acceptor moieties were chosen from commercially-available compounds with low-lying LUMO levels. Following this, the effect of the acceptor moieties was studied by photophysics, and the molecules were later implemented in electroluminescence devices.

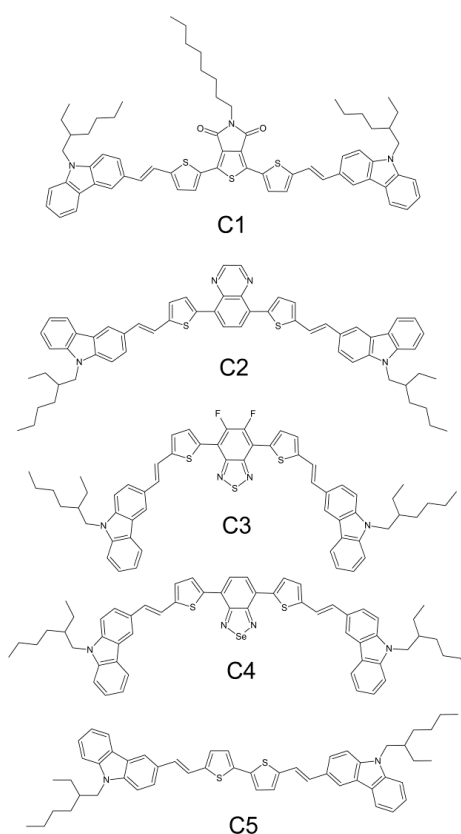


Figure 1. Chemical structures of compounds C1, C2, C3, C4 and C5.

2. Materials and Methods

2.1. Synthesis

^1H - and ^{13}C -NMR spectra were recorded on a Varian 300 MHz system (300 MHz for ^1H and 75 MHz for ^{13}C), in specified solvents using tetramethylsilane as the internal reference. The chemical shifts (δ) are reported in parts per million (ppm) and the coupling constants (J) in Hertz. HRMS analysis were performed on a Waters Xevo G2 Q-TOF mass spectrometer (Waters Corporation, MA, USA) with electrospray ionization. Anhydrous 2-ethylhexylamine (97%), DMSO, and *n*-butyllithium (2.5 M in hexane) were purchased from ACROS Organics (Thermo Fisher Scientific, Geel, Belgium) and used as obtained. Dichloromethane (DCM, for HPLC, 99.8%) and $\text{Pd}(\text{PPh}_3)_4$ were obtained from Sigma-Aldrich (Saint Louis, MO, USA), and hexanes fractionated from petroleum were obtained from Avantor Performance Materials Poland S.A. (Gliwice, Poland).

9-(2-ethylhexyl)-9H-carbazole (2): A modified procedure for the alkylation of phenols was modified from R. Motyka et al. [36]. 9H-carbazole (1) (5.0 g, 30.0 mmol) and powdered potassium hydroxide (1.85 g, 33.0 mmol) were mixed in DMSO (50 mL) under an argon atmosphere for 10 min. Then, 2-ethylhexyl bromide (97%) (5.95 g, 5.48 mL, 30.0 mmol) was added dropwise with stirring, and stirring was continued for 12 h. Water (300 mL) was added to the reaction mixture, which was then extracted with DCM (3×50 mL). The extracts were combined and washed with water and brine and then dried over anhydrous MgSO_4 . The resulting solution was evaporated, and the residue was purified using silica gel column chromatography with hexane (fractionated from petroleum 65–80 °C) as an eluent to yield 7.50 g (90% yield) of product (2) as colorless thick oil. The structure of the compound was confirmed by NMR analysis [37]. ^1H -NMR (300 MHz, CDCl_3) δ (ppm): 8.10 (m, 2H, $\text{C}_{4,5\text{Ar}}\text{-H}$), 7.51–7.42 (m, 2H, $\text{C}_{2,7\text{Ar}}\text{-H}$), 7.39 (d, $^3J = 7.7$ Hz, 2H, $\text{C}_{1,8\text{Ar}}\text{-H}$), 7.29–7.17 (m, 2H, $\text{C}_{3,6\text{Ar}}\text{-H}$), 4.35–3.97 (m, 2H, $>\text{N-CH}_2\text{-}$), 2.16–1.98 (m, 1H, $-\text{CH}<$), 1.50–1.28 (m, 8H, $4 \times -\text{CH}_2\text{-}$), and 1.00–0.75 (m, 6H, $2 \times -\text{CH}_3$).

9-(2-ethylhexyl)-9H-carbazole-3-carbaldehyde (3): Using a procedure adapted from Z. Yang et al. [38], 9-(2-ethylhexyl)-9H-carbazole (**2**) (7.40 g, 26.4 mmol), DMF (1.93 g, 2.05 mL, 26.4 mmol) and 30 mL of anhydrous CHCl₃ were placed into a dried, 50 mL round-bottom flask equipped with a magnetic stirrer and reflux condenser. The entire system was flushed with inert gas and cooled to 0 °C with vigorous stirring. To this mixture, POCl₃ (4.05 g, 2.50 mL) was added dropwise via syringe, and afterwards the cooling bath was removed, and the mixture was heated under reflux for 12 h. Next, most CHCl₃ was evaporated, and the residue was poured into ice water (100 mL), and the pH was adjusted to 7–8 by adding NaHCO₃. The aqueous suspension was extracted with CH₂Cl₂ (3 × 25 mL), and the combined extracts were washed with water several times before being dried with anhydrous MgSO₄. After CH₂Cl₂ was removed, the crude product was purified by silica gel column chromatography with hexane/DCM (2:1, *v/v*) as an eluent to afford 5.50 g (67% yield) of a pale-yellow liquid product (**3**). The structure of the compound was confirmed by NMR analysis [37]. ¹H-NMR (300 MHz, CDCl₃) δ(ppm): 10.09 (s, 1H, -CHO), 8.60 (d, ⁴J = 1.6 Hz, 1H, C_{4Ar}-H), 8.26–8.07 (m, 1H, C_{5Ar}-H), 8.00 (dd, ³J = 8.6 Hz, ⁴J = 1.6 Hz, 1H, C_{2Ar}-H), 7.53 (ddd, ³J = 8.3 Hz, ³J = 7.1 Hz, ⁴J = 1.2 Hz, 1H, C_{Ar}-H), 7.48–7.40 (m, 2H, 2 × C_{Ar}-H), 7.32 (ddd, ³J = 8.0 Hz, ³J = 7.1 Hz, ⁴J = 1.0 Hz, 1H, C_{Ar}-H), 4.39–3.91 (m, 2H, >N-CH₂-), 2.24–1.86 (sept., ³J = 6.0 Hz, 1H, -CH<), 1.54–1.08 (m, 8 H, 4 × -CH₂-), 0.92 (t, ³J = 7.4 Hz, 3H, -CH₃), and 0.85 (t, ³J = 7.1 Hz, 3H, -CH₃). ¹³C-NMR (75 MHz, CDCl₃) δ(ppm): 191.86 (-CHO), 144.68, 141.76, 128.61, 127.22, 126.79, 124.05, 123.15, 123.10, 120.80, 120.40, 109.83, 109.36, 47.85 (>N-CH₂-), 39.51, 31.12, 28.89, 24.52, 23.13, 14.12, and 11.02.

(9-(2-ethylhexyl)-9H-carbazol-3-yl)methanol (4): The synthesis was performed according to a modified procedure described by D. Barpuzary et al. [39]: 3-formyl-N-(2-ethylhexyl)carbazole (**3**) (3.92 g, 12.75 mmol) and 50 mL of dry THF were placed in a 100 mL round-bottom flask, which was purged with argon, and the contents were cooled to 0 °C. Then, with vigorous stirring, sodium borohydride (0.53 g, 14.0 mmol) was added to the mixture in small portions, and stirring was continued overnight at room temperature. Afterwards, the reaction mixture was poured into cold water and extracted several times with dichloromethane. The combined organic layers were dried using anhydrous magnesium sulphate, and the solvent was removed under vacuum. The crude product was purified by silica column chromatography using dichloromethane as an eluent to yield 3.27 g (83% yield) of (**4**) as a clear oil. ¹H-NMR (300 MHz, CDCl₃) δ(ppm): 8.16–7.96 (m, 2H, C_{Ar}-H), 7.51–7.41 (m, 2H, C_{Ar}-H), 7.41–7.29 (m, 2H, C_{Ar}-H), 7.27–7.16 (m, 1H, C_{Ar}-H), 4.81 (s, 2H, -CH₂-OH), 4.12 (d, ³J = 7.0 Hz, 2H, >N-CH₂-), 2.12–1.96 (m, 1H, -CH<), 1.87 (s, 1H, -OH), 1.50–1.11 (m, 8 H, -CH₂-), and 0.99–0.71 (m, 6 H, 2 × -CH₃).

[(9-(2-ethylhexyl)-9H-carbazol-3-yl)methyl]triphenylphosphonium bromide (5): The synthesis was performed according to a modified procedure described by D. Barpuzary et al. [39]. A 100 mL round-bottom flask with a condenser was charged with compound **4** (3.25 g, 10.5 mmol), triphenylphosphine hydrobromide (3.60 g, 10.5 mmol), and 60 mL of DCM. The mixture was heated under reflux under an inert atmosphere for 12 h. After cooling to room temperature, the product was precipitated with diethyl ether, but the precipitate was a very thick viscous liquid. Neither rubbing with a glass rod, nor precipitation using benzene instead of Et₂O yielded results. Therefore, solvent was decanted from the sticky product, and the residue, after additional evaporation and under reduced pressure (6.0 g, 90% yield) was used directly in the next reaction without further purification.

(E) & (Z)-3-(2-(5-bromothiophen-2-yl)vinyl)-9-(2-ethylhexyl)-9H-carbazole (6): This synthesis was performed based on a modified procedure from our previous publication, P. Ledwoń et al. [40] 5-bromo-2-formylthiophene (1.80 g, 9.45 mmol), compound **5** (6.00 g, 9.45 mmol), and a catalytic amount of 18-crown-6 ether (0.40 g, 1.50 mmol) were dissolved in dry methylene chloride (300 mL). Then, anhydrous potassium carbonate (4.00 g, 30.0 mmol) was added. The resulting slurry was intensely stirred and heated under reflux for 18 h under argon, then cooled, filtered, and the solvent was removed under reduced pressure. The remaining viscous brown oil was purified using silica gel chromatography, using a mixture of dichloromethane (DCM) and hexane (1:4 *v/v*) as the eluent. Column chromatography gave one main fraction containing both isomers, which after evaporation

gave 3.9 g (8.4 mmol, 90% yield) of a pale yellow solid. The obtained mixture was not separated into individual components. From the $^1\text{H-NMR}$ spectrum analysis, it was possible to determine that the obtained mixture contained an almost equimolar amount of each isomer. $^1\text{H-NMR}$ (300 MHz, CDCl_3) δ (ppm): 8.20–8.00 (m, 2H, $\text{C}_{\text{Ar-H}}$), 7.57 (dd, $^3J = 8.6$ Hz, $^4J = 1.6$ Hz, 0.5H, $\text{C}_{\text{Ar-H}}$), 7.52–7.29 (m, 4H, $\text{C}_{\text{Ar-H}}$), 7.29–7.19 (m, 1H, $\text{C}_{\text{Ar-H}}$), 7.14 (d, $^3J = 15.9$ Hz, 0.5H, $\text{H}_{\text{vinyl-isomerE}}$), 7.01 (d, $^3J = 15.9$ Hz, 0.5H, $\text{H}_{\text{vinyl-isomerE}}$), 6.95 (d, $^3J = 3.8$ Hz, 0.5H, $\text{C}_{\text{Th-H}}$), 6.87–6.71 (m, 1H, $\text{C}_{\text{Ar-H}}$), 6.61 (d, $^3J = 11.7$ Hz, 0.5H, $\text{H}_{\text{vinyl-isomerZ}}$), 4.32–3.98 (m, 2H, $>\text{N-CH}_2-$), 2.16–1.97 (m, 1H, $-\text{CH}<$), 1.48–1.17 (m, 8H, $-\text{CH}_2-$), 1.00–0.80 (m, 6H, $-\text{CH}_3$).

Stannylation procedure: A mixture of **6** (1.00 g, 2.14 mmol) in dry THF (15 mL) was cooled to -78 °C, then *n*-butyllithium (1.10 mL, 2.5 M in hexanes, 2.75 mmol) was added dropwise over a period of 1 h. After complete addition, the mixture was stirred at -78 °C for 2 h, and tributyltin chloride (95%) (0.73 g, 2.75 mmol) was added dropwise over a period of 15 min. The mixture was allowed to warm to room temperature and was stirred overnight. Then, the flask's contents were poured into a mixture of DCM and saturated ammonium chloride solution in H_2O (200 mL, 1:1 *v/v*) and vigorously shaken for 15 min. The organic layer was separated and dried using anhydrous MgSO_4 . After filtration, solvents were removed in vacuo to give 1.75 g of crude product (**7**) in the form of a light brown oil that quickly darkened in air. NMR analysis showed that the resulting oil contained a small amount of THF and around 80% of targeted compounds. Due to its very low stability, the crude product was used without further purification.

Stille reaction—main procedure: The appropriate acceptor (0.45 mmol) and toluene (10 mL) were placed in a dried 25 mL round-bottom flask equipped with a reflux condenser and inert gas inlet. The contents of the flask were vigorously stirred and purged with argon for 0.5 h. After this time, 0.79 g (1.20 mmol) of a mixture of **7** in 4 mL of degassed toluene was injected, followed by 25.0 mg (22 μmol , 5%) of $\text{Pd}(\text{PPh}_3)_4$ and 8.0 mg (44 μmol , 10%) of copper(I) iodide (CuI). The reaction mixture was heated under reflux under an inert atmosphere for 24 h. After cooling, the contents of the flask were poured into a mixture of DCM and a saturated aqueous solution of KF (200 mL, 1:1 *v/v*) and vigorously stirred for 1 h. The organic layer was separated, washed twice with deionized water (25 mL), and dried over anhydrous magnesium sulphate. After evaporation, the residue was purified using silica gel chromatography with a mixture of chloroform/hexane (fraction from petroleum, 65–80 °C), 2:1 (*v/v*), as the eluent to give a mixture of final compounds as isomers (**C1**, **C2**, **C3**, **C4**). **Isomerization:** 200 mg of the isomer mixture of each compound was dissolved in DCM (10 mL), to which trifluoroacetic acid (5 mL) was added, followed by water (2 mL). The resulting dark mixture was stirred vigorously for 30 min, after which the organic layer was separated, washed with water and diluted ammonia, and dried over magnesium sulphate. After evaporation of DCM, the resulting solid was purified by silica gel column chromatography using chloroform/hexane 2:1 (*v/v*) as the eluent. After solvent evaporation, the solid was dissolved in a minimal amount of DCM and was precipitated in methanol to give the product in the form of the most thermodynamically-stable isomer, EE.

1,3-bis(5-((E)-2-(9-(2-ethylhexyl)-9H-carbazol-3-yl)vinyl)thiophen-2-yl)-5-octyl-4H-thieno-[3,4-c]-pyrrole-4,6(5H)-dione (C1): Substrate, 1,3-dibromo-5-octyl-4H-thieno-[3 $^{\text{C-c}}$]-pyrrole-4,6(5H)-dione 0.10 g (0.24 mmol), reaction gave 225 mg of a mixture of three isomers, from which 195 mg (92% yield) of the desired product was obtained as a brown powder. Melting point: 79–81 °C. $^1\text{H-NMR}$ (300 MHz, CD_2Cl_2) δ (ppm): 8.13 (s, 2H, Carb-H4), 8.08 (d, $^3J = 7.6$ Hz, 2H, Carb-H5), 7.89 (d, $^3J = 3.9$ Hz, 2H, Th-H3), 7.57 (dd, $^3J = 8.6$ Hz, $^4J = 1.4$ Hz, 2H, Carb-H2), 7.52–7.42 (m, 2H, Carb-H6), 7.42–7.28 (m, 4H, Carb-H1,8), 7.28–7.20 (m, 2H, Carb-H7), 7.17 (s, 4H, Vinyl-H1,H2), 7.01 (d, $^3J = 3.9$ Hz, 2H, Th-H4), 4.08 (d, $^3J = 7.1$ Hz, 4H, $>\text{N-CH}_2-$), 3.58 (t, $^3J = 7.4$ Hz, 2H, $>\text{N-CH}_2-$), 2.18–1.90 (m, 2H, $-\text{CH}<$), 1.78–1.60 (m, 2H, $-\text{CH}_2-$), 1.49–1.12 (m, 26H, $-\text{CH}_2-$), and 1.03–0.76 (m, 15H, $-\text{CH}_3$). $^{13}\text{C-NMR}$ (75 MHz, CD_2Cl_2) δ (ppm): 162.75, 147.49, 141.75, 141.37, 136.10, 131.84, 131.02, 130.62, 128.58, 127.92, 126.73, 126.24, 124.78, 123.51, 123.04, 120.61, 119.46, 119.04, 118.53, 109.75, 109.69, 47.84, 39.78, 38.77, 32.22, 31.37, 29.62, 29.16, 28.90, 27.40, 24.78, 23.42, 23.04, 14.24, 14.14, and 11.04.

MALDI-TOF MS calculated mass for $C_{66}H_{74}N_3O_2S_3 + [M+H]^+$: 1036 (100%), 1037 (76%), and 1039 (42%) found: 1036 (100%), 1037 (77%), and 1039 (40%).

5,8-bis(5-(*E*)-2-(9-(2-ethylhexyl)-9*H*-carbazol-3-yl)vinyl)thiophen-2-yl)quinoxaline (C2): The substrate–5,8-dibromoquinoxaline 0.15 g (0.52 mmol), reaction gave 427 mg of a mixture of isomers, from which 365 mg (78% yield) of the desired product was obtained as a brown powder. Melting point: 135–137 °C. **1H -NMR** (300 MHz, $CDCl_3$) δ (ppm): 9.01 (s, 2H, Quin–H2,H3), 8.22 (d, $J = 1.4$ Hz, 2H, Quin–H6,H7), 8.18–8.06 (m, 4H, Carb–H4,H5), 7.77 (d, $^3J = 3.9$ Hz, 2H, Th–H3), 7.65 (dd, $^3J = 8.6$ Hz, $^4J = 1.6$ Hz, 2H, Carb–H2), 7.55–7.43 (m, 2H, Carb–H6), 7.43–7.33 (m, 4H, Carb–H1,8), 7.31 (s, 4H, Vinyl–H1,H2), 7.29–7.20 (m, 2H, Carb–H7), 7.14 (d, $^3J = 3.9$ Hz, 2H, Th–H4), 4.15 (d, $^3J = 7.0$ Hz, 4H, >N–CH₂–), 2.22–1.92 (m, 2H, –CH<), 1.52–1.16 (m, 16H, –CH₂–), 0.92 (t, $^3J = 7.4$ Hz, 6H, –CH₃), and 0.87 (t, $^3J = 7.0$ Hz, 6H, –CH₃). **^{13}C -NMR** (75 MHz, $CDCl_3$) δ (ppm): 146.73, 143.37, 141.45, 140.87, 139.96, 136.58, 131.77, 129.85, 128.33, 127.83, 127.23, 125.92, 125.49, 124.39, 123.33, 122.94, 120.50, 119.55, 119.15, 118.70, 109.37, 109.31, 47.65, 39.56, 31.14, 28.95, 24.53, 23.19, 14.18, and 11.05. **HRMS** (ESI) calculated mass for $C_{60}H_{60}N_4S_2^+ [M]^+$: 900.4259, found: 900.4296; $C_{60}H_{61}N_4S_2^+ [M+H]^+$: 901.4332 (100.0%), 902.4366 (64.9%), and 903.4399 (20.7%), found: 901.4333 (100%), 902.4351 (50%), and 903.4368 (30%).

4,7-bis(5-(*E*)-2-(9-(2-ethylhexyl)-9*H*-carbazol-3-yl)vinyl)thiophen-2-yl)-5,6-difluorobenzo[*c*]-[1,2,5]-thiadiazole (C3): Substrate–4,7-dibromo-5,6-difluorobenzo[1,2,5]thiadiazole 0.15 g (0.45 mmol), reaction gave 320 mg of a mixture of isomers, from which 280 mg (66% yield) of desired product was obtained as a dark brown powder. Melting point: 237–239 °C. **1H -NMR** (300 MHz, $CDCl_3$) δ (ppm): 8.31–8.18 (m, 4H, Carb–H4, Th–H3), 8.13 (d, $^3J = 7.6$ Hz, 2H, Carb–H5), 7.66 (dd, $^3J = 8.6$ Hz, $^4J = 1.3$ Hz, 2H, Carb–H2), 7.54–7.43 (m, 2H, Carb–H6), 7.43–7.23 (m, 10H, Carb–H1,7,8, Vinyl–H1,2), 7.21 (d, $^3J = 4.0$ Hz, 2H, Th–H4), 4.16 (d, $^3J = 6.9$ Hz, 4H, >N–CH₂–), 2.16–1.96 (m, 2H, –CH<), 1.47–1.15 (m, 16H, –CH₂–), and 1.01–0.76 (m, 12H, –CH₃). **^{13}C -NMR** (150 MHz, $CDCl_3$) δ (ppm): 150.02, 149.07, 147.74, 147.18, 144.81, 141.51, 131.92, 126.06, 125.87, 124.53, 123.38, 122.91, 120.54, 119.29, 118.91, 109.41, 109.37, 47.70, 39.59, 31.18, 28.99, 24.57, 23.20, 14.20, and 11.06. Not all of the carbon signals are visible in the spectrum due to the extremely low solubility of the compound and the presence of fluorine atoms in its structure, the coupling of which with the ^{13}C carbon nuclei additionally splits and reduces the size of recorded signals. **HRMS** (ESI) calculated mass for $C_{58}H_{56}F_2N_4S_3^+ [M]^+$: 942.3635, found: 942.3627; $C_{58}H_{57}F_2N_4S_3^+ [M+H]^+$: 943.3708 (100.0%) and 944.3741 (62.7%), found: 943.3697 (100%) and 944.3669 (60%).

4,7-bis(5-(*E*)-2-(9-(2-ethylhexyl)-9*H*-carbazol-3-yl)vinyl)thiophen-2-yl)benzo[*c*][1,2,5]selenadiazole (C4): Substrate–4,7-dibromobenzo[*c*][1,2,5]selenadiazole 0.15 g (0.44 mmol), reaction gave 220 mg of a mixture of three isomers, from which 190 mg (45% yield) of desired product was obtained as a dark blue powder. Melting point: 139–141 °C. **1H -NMR** (300 MHz, CD_2Cl_2) δ (ppm): 8.22 (d, $^4J = 1.5$ Hz, 2H, Carb–H4), 8.13 (d, $^3J = 7.6$ Hz, 2H, Carb–H5), 8.01 (d, $^3J = 3.9$ Hz, 2H, Th–H3), 7.80 (s, 2H, BSeD–H5), 7.66 (dd, $^3J = 8.7$ Hz, $^4J = 1.5$ Hz, 2H, Carb–H2), 7.53–7.45 (m, 2H, Carb–H6), 7.44–7.38 (m, 4H, Carb–H1,8), 7.34 (d, $^3J = 16.1$ Hz, 2H, Vinyl–H1), 7.30–7.20 (m, 4H, Vinyl–H2, Carb–H7), 7.16 (d, $^3J = 3.9$ Hz, 2H, Th–H4), 4.17 (d, $^3J = 7.1$ Hz, 4H, >N–CH₂–), 2.17–1.97 (m, 2H, –CH<), 1.49–1.15 (m, 16H, –CH₂–), 0.92 (t, $^3J = 7.4$ Hz, 6H, –CH₃), and 0.86 (t, $^3J = 7.1$ Hz, 6H, –CH₃). **^{13}C -NMR** (75 MHz, CD_2Cl_2) δ (ppm): 158.54, 145.73, 141.82, 141.28, 138.18, 130.39, 128.62, 128.43, 127.37, 126.65, 126.26, 125.73, 124.71, 123.57, 123.11, 120.67, 119.53, 119.45, 118.83, 109.85, 109.75, 47.95, 39.85, 31.43, 29.23, 24.84, 23.47, 14.18, and 11.10. **HRMS** (ESI) calculated mass for $C_{58}H_{58}N_4S_2Se^+ [M]^+$: 954.3268 (100%), 955.3302 (63%), and 952.3276 (48%), found: 954.3224 (100%), 955.3277 (75%), and 952.3361 (60%).

5,5'-bis(*E*)-2-(9-(2-ethylhexyl)-9*H*-carbazol-3-yl)vinyl)-2,2'-bithiophene (C5): The product was obtained in the homo-coupling side reaction of compound 7 when the preparation of compound C2 was carried out in DMF using a procedure described by J. E. Baldwin et al. [41]. In this reaction, 0.65 g (0.96 mmol) of 9-(2-ethylhexyl)-3-(2-(5-(tributylstannyl)thiophen-2-yl)vinyl)-9*H*-carbazole (7) was used, and after purification, 150 mg of product C5 was isolated in the form of an orange solid in 40% yield. Melting point: 168–170 °C. **1H -NMR** (300 MHz, $CDCl_3$) δ (ppm): 8.18 (d, $^4J = 1.5$ Hz, 2H,

Carb-H4), 8.12 (d, $^3J = 7.7$ Hz, 2H, Carb-H5), 7.61 (dd, $^3J = 8.7$ Hz, $^4J = 1.5$ Hz, 2H, Carb-H2), 7.53–7.42 (m, 2H, Carb-H6), 7.42–7.30 (m, 4H, Carb-H1,H8), 7.30–7.22 (m, 2H, Carb-H7), 7.23 (d, $^3J = 15.9$ Hz, 2H, Vinyl-H1), 7.10 (d, $^3J = 15.9$ Hz, 2H, Vinyl-H2), 7.10 (d, $^3J = 3.8$ Hz, 2H, Th-H), 6.97 (d $^3J = 3.8$ Hz, 2H, Th-H), 4.16 (d, $^3J = 7.1$ Hz, 4H, >N-CH₂-), 2.19–1.92 (m, 2H, -CH<), 1.50–1.12 (m, 16H, -CH₂-), 0.92 (t, $^3J = 7.5$ Hz, 6H, -CH₃), 0.87 (t, $^3J = 7.1$ Hz, 6H, -CH₃). **¹³C-NMR** (75 MHz, CDCl₃) δ(ppm): 142.78, 141.46, 140.89, 135.63, 129.67, 128.14, 126.37, 125.94, 124.37, 124.03, 123.34, 122.93, 120.50, 119.19, 119.17, 118.61, 109.38, 109.31, 47.67, 39.56, 31.15, 28.95, 24.54, 23.18, 14.17, 11.04. **HRMS** (ESI) calculated mass for C₅₂H₅₆N₂S₂⁺ [M]⁺: 772.3885, found: 772.3898; C₅₂H₅₇N₂S₂⁺ [M + H]⁺: 773.3958 (100.0%), 774.3991 (56.2%), and 775.4025 (15.5%), found: 773.3945 (100%), 774.3951 (50%), and 775.3914 (12%).

2.2. Electrochemistry

Cyclic voltammetry experiments were carried out on a classic three-electrode assembly with a Pt wire as the working electrode, a Pt spiral as the counter electrode, and Ag as the pseudoreference electrode on an Autolab PGSTATM101 potentiostat (Metrohm Autolab B.V., Utrecht, The Netherlands). The potential was calibrated versus a ferrocene/ferrocinium redox couple as an internal standard. Experiments were performed in dichloromethane (DCM) (Sigma-Aldrich, Chromasolv for HPLC) with 0.1 M tetrabutylammonium tetrafluoroborate (98%, Tokyo Chemical Industry Co., Nihonbashi-honcho, Japan) as the supporting electrolyte. All solutions were deaerated with Ar before measurements. Ionization potential (*IP*) was estimated from equation:

$$IP = |e^-|(5.1 + E_{ox\ onset}) \quad (1)$$

Electron affinity (*EA*) was estimated from the equation:

$$EA = |e^-|(5.1 + E_{red\ onset}) \quad (2)$$

Electrochemical band gap (ΔE_{gel}) was estimated from the equation:

$$\Delta E_{gel} = IP - EA \quad (3)$$

2.3. Photophysics

UV-Vis absorption spectra of dilute solutions ($\sim 10^{-5}$ M) and thin films were recorded on a Cary 5000 (Varian) spectrometer. Photoluminescence spectra of studied samples were performed at room temperature with an Edinburgh Instruments FLS980 fluorescence spectrometer (Edinburgh Instruments Ltd., Livingston, UK) with a Xe-lamp as an excitation source and an R-928 photomultiplier detector. The photoluminescence quantum yields (PLQY) of compounds were measured using an integrating sphere from Edinburgh Instruments with a BENFLEC interior coating. Fluorescence lifetimes of dilute solutions were acquired by time-correlated single photon counting (TCSPC) methods on an Edinburgh Instruments FLS980 fluorescence spectrometer.

2.4. Devices

OLEDs were fabricated by a hybrid spin-coating/evaporation method. The size of the pixels was 4.5 mm². PEDOT:PSS (poly(3,4-ethylenedioxythiophene)-poly(styrenesulfonate), Heraeus Hanau, Germany) was used as a hole injection layer (HIL), and blends of PVK (Poly(9-vinylcarbazole), M_w: 25,000–50,000) and PO-T2T (2,4,6-tris[3-(diphenylphosphinyl)phenyl]-1,3,5-triazine) doped with dyes were used as an emitting layer. Evaporated thin layers of PO-T2T were introduced as hole blocking layers (HBLs) and electron transport layers (ETLs). Cesium carbonate (Cs₂CO₃) and aluminum were used as the cathode. OLED devices were made on pre-cleaned and patterned indium-tin-oxide (ITO) substrates with a sheet resistance of 20 Ω/sq and an ITO thickness of 100 nm (Ossila Ltd, Sheffield, UK). PEDOT:PSS was spin-cast and annealed on a hotplate at 150 °C for 10 min to obtain 40 nm thin films. The active layers were spin-cast from chloroform solutions of PVK:PO-T2T (60:40 *w/w*) (12 mg/mL)

with 8 wt% of dopant and then annealed at 60 °C for 20 min under a nitrogen atmosphere. All solutions were filtered before use with a PVDF or PTFE syringe filter with a 0.45 µm pore size. 50 nm layers of PO-T2T and cathode layers were thermally evaporated using a Prevac deposition system under a pressure of 10⁻⁶ mbar. An organic semiconductor (PO-T2T) and aluminum were deposited at a rate of 1 Ås⁻¹, and the Cs₂CO₃ layer was deposited at a rate of 0.1–0.2 Ås⁻¹. The thickness and roughness of the organic layers were controlled by a Bruker Dektak XT profilometer (Bruker Corporation, Billerica, Massachusetts, USA). The device characteristics were recorded using a Minolta CS-200 camera connected with a Keithley 2400 source measurement unit (Tektronix, Beaverton, Portland, OR, USA), whereas the electroluminescence spectra were recorded by Ocean Optic USB2000 and StellarNet SILVER-Nova Super Range TEC spectrometers. All materials were purchased from Sigma Aldrich (Saint Louis, MO, USA) or Lumtec (Luminescence Technology Corp., New Taipei City, Taiwan).

3. Results

3.1. Synthesis

The emissive materials were obtained by Stillecoupling between different acceptor units and stannylated D-π arm-containing thiophene vinyl and carbazole units. D-π arms were obtained via the multistep synthetic route shown in Figure 2.

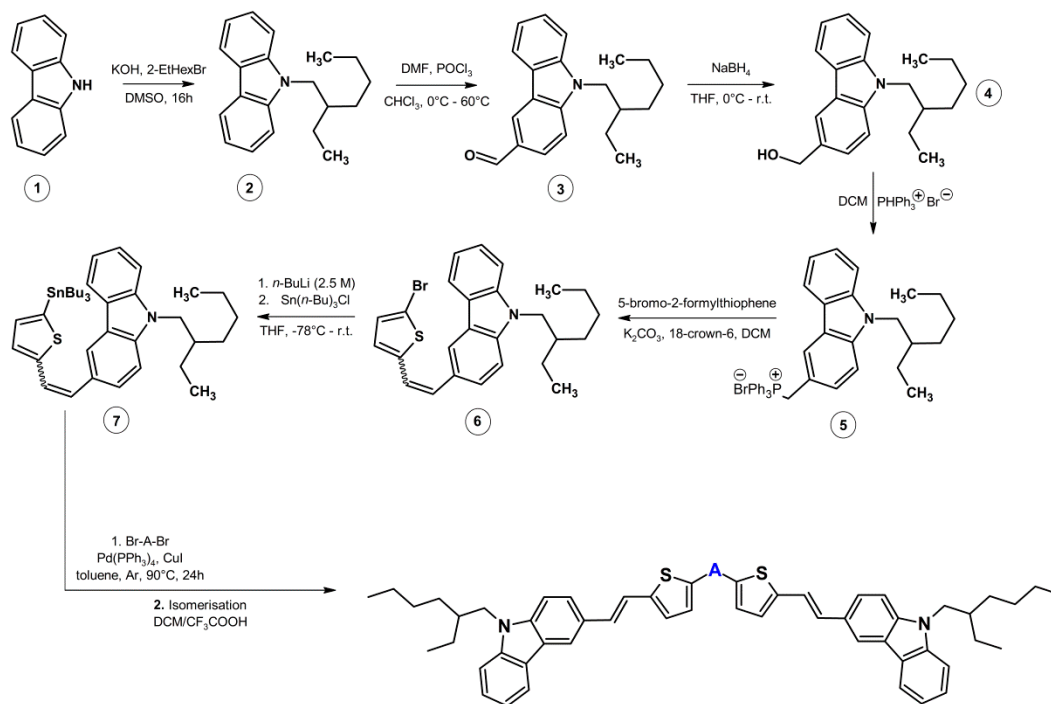


Figure 2. Synthesis procedure.

The first step of the synthesis was performed where the nitrogen atom of 9*H*-carbazole (1) was alkylated by a nucleophilic substitution reaction (S_N2). Next, the obtained alkylcarbazole (2) was formylated using the Vilsmeier–Haack reaction, and the resulting aldehyde (3) was reduced using sodium borohydride to yield the alcohol (4). This alcohol was converted to a phosphonium salt (5) using triphenylphosphine hydrobromide, and the resulting product (5) was condensed with 5-bromo-2-formylthiophene through a Wittig reaction to obtain a vinyl bond between the carbazole and thiophene units. 3-(2-(5-bromothiophen-2-yl)vinyl)-9-(2-ethylhexyl)-9*H*-carbazole (6) was formed only when a weak base was used (K₂CO₃), and all attempts using stronger bases, such as MeONa or *t*-BuOK were unsuccessful. The Wittig reaction gave compound 6 as a mixture of two isomers (*E* and *Z*) which were not separated into individual components, and were used in such a form in

the next stages. Both isomers were converted into their stannyl derivatives (**7**) by two subsequent reactions: Halogen-lithium and lithium-tin exchange. The final stage involved Stille cross-coupling and isomerization of vinyl bonds to give the most thermodynamically-stable isomer (*E,E*) of the final products (**C1**, **C2**, **C3**, and **C4**). It is also worth noting that the last step must be performed in a nonpolar solvent (e.g., toluene) because when the reaction was carried out in polar solvents such as DMF, compound **C5** was the main product, which is a product of the homo-coupling of compound **7**. All the final compounds except **C3** show good solubility in common organic solvents, such as DCM, toluene, and chloroform.

3.2. Electrochemical Properties

All studied compounds contained two identical electron-donor moieties and different electron-acceptor units. Electrochemical measurements were used to estimate the influence of these units using cyclic voltammetry (CV) in a DCM/ Bu_4NBF_4 electrolyte, and the results are shown in Figure 3 and summarized in Table 1. All samples showed quasi-reversible reduction peaks. The reduction onset potential ($E_{\text{red onset}}$) varied from -1.42 V to -1.76 V, depending on the central electron-acceptor unit. The reduction of the reference compound **C5** was recorded at -2.25 V. The results are in good agreement with other donor-acceptor compounds in which the type of electron-deficient unit determined the reduction behavior and the energy of the LUMO (E_{LUMO}) [7,42,43]. The reduction was related to the insertion of an electron into the LUMO [44,45].

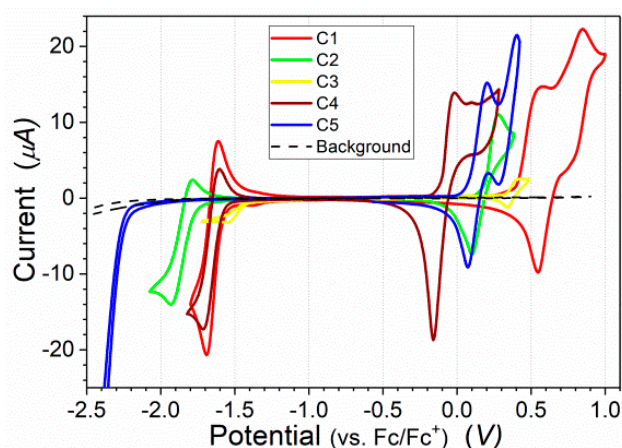


Figure 3. Cyclic voltammetry of 4 mM solutions of **C1**, **C2**, **C4**, **C5** or a saturated solution of **C3** in DCM/ Bu_4NBF_4 electrolyte, at a potential sweep rate of 50 mV/s.

Table 1. Electrochemical and optical properties.

Compound	¹ $E_{\text{ox onset}}$ [V]	² $E_{\text{red onset}}$ [V]	³ IP [eV]	⁴ EA [eV]	⁵ E_{HOMO} [eV]	⁵ E_{LUMO} [eV]	⁶ ΔE_{gel} [eV]	⁷ ΔE_{opt} [eV]
C1	0.4	-1.58	5.50	3.52	-5.50	-3.52	1.98	2.03
C2	0.18	-1.76	5.28	3.34	-5.28	-3.34	1.94	1.86
C3	0.34	-1.42	5.44	3.68	-5.44	-3.68	1.76	1.85
C4	-0.12	-1.59	4.98	3.51	-4.98	-3.51	1.47	1.65
C5	0.08	-2.25	5.18	2.85	-5.18	-2.85	2.33	2.27

¹ $E_{\text{ox onset}}$ is the onset oxidation potential; ² $E_{\text{red onset}}$ is the onset reduction potential; ³ IP is the ionization potential estimated from the equation $IP = |e^-(5.1 + E_{\text{ox onset}})|$; ⁴ EA is the electron affinity estimated from the equation $EA = |e^-(5.1 + E_{\text{red onset}})|$; ⁵ E_{HOMO} and E_{LUMO} were electrochemically-estimated approximate values of the HOMO and LUMO energy; ⁶ ΔE_{gel} is the electrochemical band gap, calculated from $\Delta E_{\text{gel}} = IP - EA$; and ⁷ E_{gopt} is the optical band gap, as estimated from the edges of electronic absorption spectra of thin films.

Analyzing the CV curves in the oxidation range revealed large differences between the compounds. The oxidation onset potential ($E_{\text{ox onset}}$) ranged from -0.12 V for **C4** up to 0.4 V for **C1**. The large difference of $E_{\text{ox onset}}$ between these two similar compounds exceeded 0.5 V, while both compounds

exhibited nearly the same $E_{\text{red onset}}$. The large differences in $E_{\text{ox onset}}$ in all studied compounds clearly indicates that electron-acceptor units have a significant impact on the energy of the HOMO (E_{HOMO}), which determines properties such as the IP and oxidation behavior.

$E_{\text{red onset}}$ and $E_{\text{ox onset}}$ were used to estimate the electrochemical EA and IP (Figure 4) [46]. The values of electrochemically-estimated EA , IP , E_{HOMO} , and E_{LUMO} are summarized in Table 1. The acceptor units affected both IP and EA , and the analysis of the electrochemical results revealed that the acceptor unit significantly altered IP and E_{HOMO} . The direction of the changes was different for different acceptors. In compounds **C1**, **C2**, and **C3**, the HOMO was stable compared with **C5**, while **C4** showed a much higher E_{HOMO} value. **C4**, which contained a benzselenadiazole unit, exhibited an IP shift of 4.98 eV. These results clearly indicate the unusual properties of benzselenadiazole, which simultaneously increased E_{HOMO} and lowered E_{LUMO} , leading to low molecular weight material with a narrow energy gap (ΔE_{gel}) of 1.47 eV. Compared with other donor–acceptor π -conjugated molecules, such a narrow ΔE_{gel} is usually only seen in highly-conjugated polymers [47–50]. The results reveal the potentially beneficial properties of benzselenadiazole-based conjugated materials, and these results are in good agreement with other research [51–56].

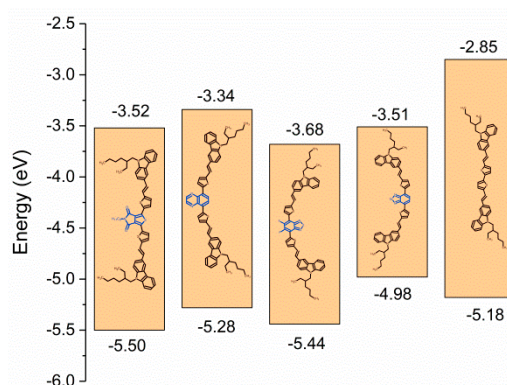


Figure 4. Energy diagram of compounds **C1–C5**.

3.3. Photophysical Properties

The normalized optical absorption spectra of toluene solutions and spin-coated thin films of the studied materials are shown in Figure 5. Molecules showed two main absorption regions: The main lower-energy bands from 451–583 nm and higher-energy bands from 200–300 nm and 350–550 nm (Table 2). The absorption spectra of the studied materials were clearly correlated with their donor–acceptor–donor (D–A–D) structures, where 9-(2-ethylhexyl)-9H-carbazole was introduced as a donor unit linked with different acceptors by a π -linker. All molecules exhibited high-energy absorption bands centered in the 200–340 nm region (Figure 5b), which was correlated with the absorption of the carbazole moiety [57,58]. The **C5** and **C1** spectra look similar, with one main band located at 451 nm in **C5** which is red-shifted in the **C1** spectrum. This absorption band was attributed mainly to the bithiophene core of the molecules [59]. Molecules **C2**, **C3**, and **C4** showed dual-band absorption profiles with their lowest-energy absorption peaks positioned at 520 nm, 539 nm, and 583 nm, respectively. These peaks originated mainly from an extensive π -conjugated system involving the acceptor moiety quinoxaline core [60], difluoro-2,1,3-benzothiadiazole [61,62], and 2,1,3-benzoselenadiazole [63,64]. The red shift observed in the lowest-energy absorption band of **C4** correlated closely with the electrochemical results, and is explained by a decrease in the degree of aromaticity in the acceptor unit when the sulphur was replaced with selenium [65]. This destabilized the HOMO and simultaneously stabilized the LUMO, which led to a red-shift in the absorption spectrum.

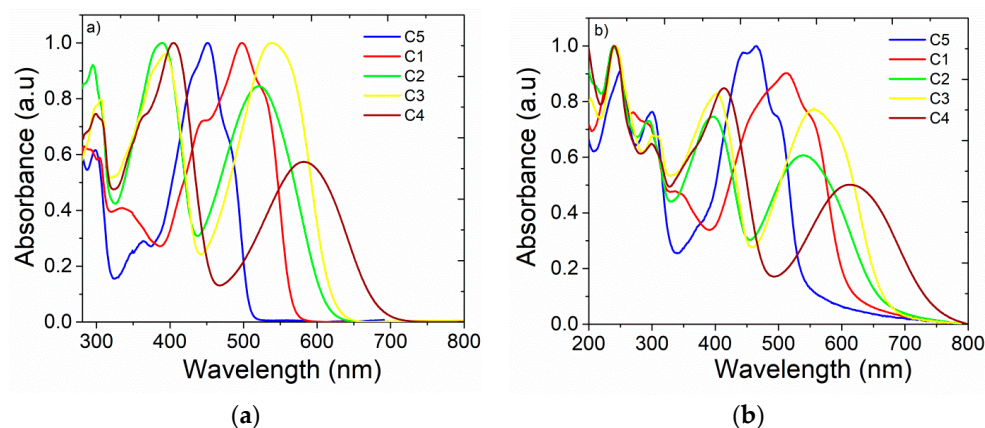


Figure 5. Normalized absorption spectra of dilute solutions (10^{-5} M in toluene) (a), and spin-coated thin films (b) of the compounds.

Table 2. The photophysical properties of C1–C5 in dilute solution (10^{-5} M in toluene, chloroform, THF, and DCM) and in the solid state.

	$\lambda_{\text{abs,tol}}$ [nm]	$\lambda_{\text{abs,film}}$ [nm]	$\lambda_{\text{PLzeon.}}$ [nm]	$\lambda_{\text{PL,tol}}$ [nm]	$\lambda_{\text{PL,chlor}}$ [nm]	$\lambda_{\text{PL,THF}}$ [nm]	$\lambda_{\text{PL,DCM}}$ [nm]	λ_{PLfilm} [nm]
C5	451	465	502	505	509	506	510	528
C1	498	514	560	568	582	585	592	685
C2	520	540	633	651	670	675	679	725
C3	539	558	640	660	695	701	707	740
C4	583	614	733	740	770	776	782	835

It has been suggested in works devoted to the photophysics of D–A type molecules that the low-energy band of the absorption spectrum arises due to intramolecular charge transfer [66,67]. Therefore, the absorption and emission spectra of studied compounds were obtained in solvents with different polarities, and the absorption spectra remained unchanged (Figure S16), which may suggest that polarity doesn't affect the energy of ground states.

The solid-state absorption spectra displayed a red shift compared with spectra in dilute solutions due to interactions between molecules occurring in neat films. From the long wavelength absorption edge of the UV–VIS spectra in the solid state, the optical band gaps of emitters were estimated. The E_g values are given in Table 1, where it was noticed that different molecular cores influenced optical properties of studied D–A–D compounds, such as optical band gaps and as a consequence the color of emitted light can be tuned (Figure 6).

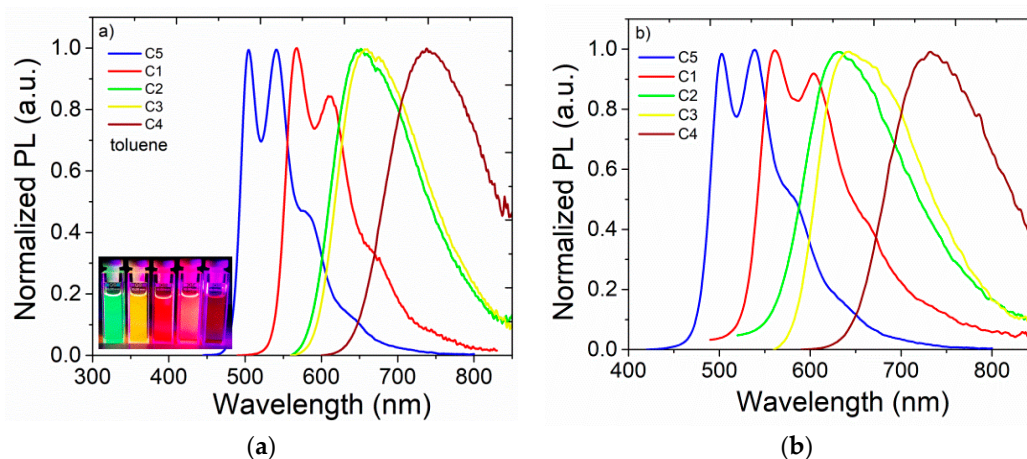


Figure 6. Normalized photoluminescence (PL) spectra of the dilute solutions (10^{-5} M in toluene) (a), and 1 wt% of emitters in a zeonex matrix (spin-coated thin films) (b).

The photoluminescence (PL) spectra of compounds in toluene solution and a zeonex matrix are shown in Figure 6, and the photoluminescence maxima and photoluminescence quantum yields (PLQY) in different solvents are collated in Table 2. The designed molecules showed fluorescence with a large Stokes shift, which covered a broad part of the spectrum from the green to near-infrared regions. A vibronic structure of the fluorescence spectra of **C5** and **C1** in toluene was observed, with emission bands centered at 505 nm, 541 nm, and 580 nm for **C5** and emission maxima at 568 nm, 612 nm, and 665 nm for **C1**. In contrast, molecules **C2**, **C3**, and **C4** displayed one broad main band with emission maxima at 651 nm, 660 nm, and 740 nm, respectively (Figure 6a, Table 2). These results, together with the Stokes shift, much smaller in the case of **C1** and **C5** molecules, may suggest more rigid structure, and smaller geometry and electronic density distribution changes during the excitation in the two molecules. However, in a non-polar rigid medium (zeonex), these emitters demonstrated blue-shifted emission in comparison to the emission observed in solvent. This rigidochromic effect suggests the intramolecular charge transfer (CT) character of the emissive state, which seems to be confirmed by the solvatochromism experiment. All molecules except **C5** displayed a positive solvatochromic effect where the emission spectra shifted to a longer wavelength as the solvent polarity increased (Table 2, Figure S16). Meanwhile, the PL spectra of the neat films (Figure S17) exhibited a strong red shift and a high amount of excited state quenching, due to strong intermolecular interactions. The PL spectra of **C5** did not change significantly when the molecule was placed in different environments. This may suggest that excitation did not change the dipole moment in molecules without an acceptor unit, and a CT state was not created. Moreover, in the case of **C5**, the highest photoluminescence quantum yield was determined to be practically independent of solvent nature (Table 3).

Table 3. Photoluminescence quantum yield (Φ_{PL}), lifetime (τ ns) and radiative, non-radiative constants of fluorescence for C1–C5 in diluted solution.

Mol	Solvent	Φ_{PL} , %	τ ns	Radiative Rate Constant, (10^9 s^{-1})	Non-Radiative Rate Constant, (10^9 s^{-1})
C5	TOL	52	0.9	0.57	0.54
	CHL	42	0.8	0.52	0.75
	DCM	50	0.9	0.56	0.56
	THF	52	0.9	0.58	0.53
C1	TOL	48	1.3	0.37	0.40
	CHL	48	1.2	0.40	0.43
	DCM	42	1.1	0.38	0.52
	THF	41	1.1	0.37	0.54
C2	TOL	34	1.9	0.17	0.35
	CHL	33	2.1	0.16	0.32
	DCM	31	1.9	0.16	0.36
	THF	32	2.1	0.15	0.32
C3	TOL	45	2.3	0.20	0.24
	CHL	45	2.9	0.16	0.16
	DCM	38	2.5	0.15	0.25
	THF	39	2.7	0.14	0.23
C4	TOL	17	2.2	0.07	0.34
	CHL	7	1.1	0.06	0.75
	DCM	4	1.0	0.04	0.95
	THF	7	1.5	0.047	0.62

Fluorescence decay measurements (Figure S18) were performed for dilute solutions at room temperature. The decay profiles were observed to occur on the nanosecond scale, which was assigned to fluorescence emission. The summarized lifetime (τ) values of the molecules in dilute toluene, chloroform, DCM, and THF are given in Table 3. It should be noticed that for compounds **C1**, **C2**, **C3**,

and **C4**, it was difficult to fit the emission decay with a monoexponential function, where a very small contribution of the second time was detected. The origin of it is unclear. However, in the case of the compound **C5**, emission decayed monoexponentially (for details, see Figure S18 and Table S1). It can be seen that the radiative rate constant, obtained from the PLQY/ τ ratio, systematically decreased upon passing from **C5**, **C1**, **C3**, **C2**, to **C4**. Evidently, the introduction of a selenium atom in the acceptor unit decreased the radiative rate constant. Such behavior may be interpreted in terms of relative twisting of the donor and acceptor moieties in the excited state. It is generally known that the radiative rate constant is a function of the twist angle (Θ) and decreases when the value of Θ changes from 0° to 90° , where the two moieties involved in the charge transfer are orbitally decoupled and, as a consequence, the transition is forbidden and k_r becomes very small. However, additional experiments and/or calculations are needed to confirm this hypothesis. On the other hand, the very low emission quantum yield observed for **C4** could be related to activation of some radiation-less processes. One of them could be an intersystem crossing phenomenon induced by a spin-orbit coupling enhancement, produced by a heavy atom. Additionally, it is known that in long-wavelength emitters, enhanced internal conversion is responsible for quenching emissive states [68].

To reduce the effects of concentration quenching and to evaluate the potential use of low concentrations of doping complexes for solution-processed OLEDs, exciplex hosts were used. Exciplex forming blend of donor and acceptor materials have been used as efficient hosts for fluorescent emitters. Such systems provide efficient charge carrier balance, which results in a long and stable operating lifetime of OLEDs [69]. Recently, Pander et al. reported a novel TADF exciplex comprised of a PVK polymer (donor) and a PO-T2T acceptor, and its further application in solution-based OLEDs [70]. The corresponding exciplex was used as a host for synthesized molecules. Moreover, the emission of a green PVK:PO-T2T exciplex overlapped with the absorption spectra of synthesized complexes, which is necessary for efficient Förster resonance energy transfer (FRET) (Figure S19) [71]. Much better matching of these spectra was observed in the case **C2**, **C3**, and **C4**, and the largest overlap was achieved by **C4**. The photoluminescence spectra of thin films of PVK:PO-T2T doped with 1, 2, 5, 8, and 10 wt% of studied compounds are shown in Figure S20 and Figure 7a. The studied materials exhibited similar behavior, and at a low doping concentrations, the PL spectra contained two emission peaks responsible for PVK:PO-T2T exciplex emission (530 nm) and dopant fluorescence (Figure S20). Complete energy transfer was achieved at 8 and 10 wt% emitter doping concentrations in PVK:PO-T2T. Interestingly, as the dopant concentration increased in the exciplex, a bathochromic shift was observed in the PL spectra (Figure S20). Additionally, the photoluminescence quantum yields of all thin films were similar and were in the range 4–5%, which suggests strong concentration-induced quenching in the solid state.

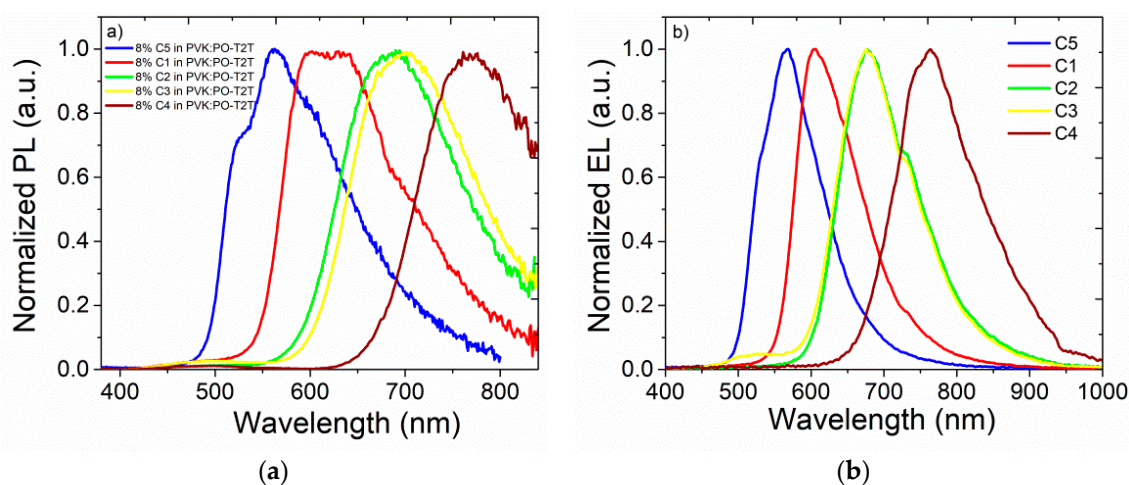


Figure 7. Photoluminescence spectra of 8 wt% **C1**–**C5** doped in PVK:PO-T2T host (a), and the electroluminescence spectra of fabricated OLEDs (b).

3.4. Device Fabrication

To unlock the potential of study's materials, they have been implemented in OLEDs. Since C1–C5 were designed and synthesized for solution-processable techniques, they were incorporated as emitting species in the polymer light-emitting diodes. The structure of the OLED prototypes were as follows: ITO/PEDOT:PSS (40 nm)/8 wt% (C1–C5) in PVK:PO–T2T (80 nm)/PO–T2T (50 nm)/Cs₂CO₃ (2 nm)/Al (100 nm). The first layer of PEDOT:PSS (poly(3,4-ethylenedioxythiophene)-poly(styrenesulfonate)) was used as a hole injection layer and was spin cast on ITO substrates from an aqueous solution. Next, the active layer consisted of a blend of low-molecular-weight PVK (Poly(9-vinylcarbazole)) and PO–T2T (2,4,6-tris[3-(diphenylphosphinyl)phenyl]-1,3,5-triazine) doped with 8 wt% of the respective molecules was spin coated on the PEDOT:PSS layer from chloroform solution. A ratio of 60:40 of PVK:PO–T2T was chosen to ensure balanced charge carrier transport to the emitters. The doping concentrations of C1–C5 were chosen due on the base of photophysical studies to guarantee complete energy transfer from the exciplex (PVK: PO–T2T) host to the emitters. Active three-component layers were spin coated by a chloroform solution on the PEDOT:PSS layer. Such polymer light-emitting layers have a good film-forming property, good carrier transporting characteristics, and can be easily processed by different solution-processable techniques (e.g., inkjet printing and slot die coating). Furthermore, a thermally-evaporated 50 nm layer of PO–T2T was introduced as an electron transport layer.

The OLED characteristics are presented in Figure 8, and the energy levels of organic semiconductors used in the devices are inserted in Figure 8a. The normalized electroluminescence (EL) spectra of OLEDs (Figure 7b) showed main emissive bands centered at 565 nm, 602 nm, 680 nm, 680 nm, and 765 nm for devices based on C5, C1, C2, C3, and C4, respectively. EL was observed in a large part of the spectrum, from green to near-infrared emission, and did not contain emission from additional layers or from the host. This indicated that excitons were fully transferred from the host to the emissive species, or the charge carriers' trapping process plays important role. Nevertheless, fabricated devices exhibited high current density at high voltage operation regimes (Figure 8a). It should be explained that OLEDs prototypes contained only three organic layers; the introduction of additional layers, such as an electron-blocking one, can improve charge carrier balance and current density characteristics.

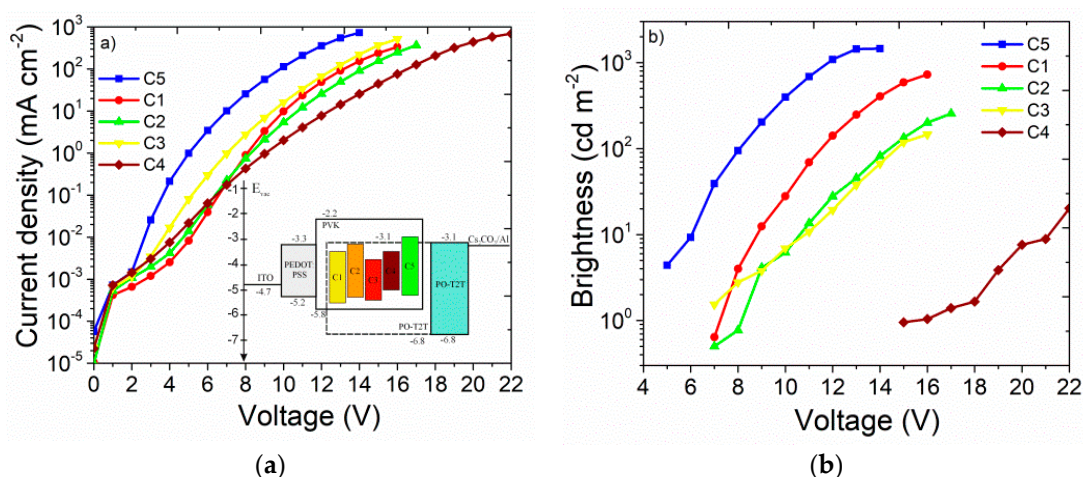


Figure 8. Current density–voltage (insert—energy band diagram of OLEDs) (a), and luminance–voltage characteristics (b) of fabricated devices.

OLEDs made with C5 emitter showed a rather low turn-on voltage (V_{on}) of 5 V, compared with OLEDs made from C1–C3 emitters, which had turn-on voltages of 7 V, and for near-infrared C4 molecule, –15 V (Figure 8b). The best performance in this work displayed the green solution processed OLEDs with the C5 molecule; the maximum brightness (L_{max}) and maximum current efficiency ($\eta_{L,max}$) were 1452 cd m⁻² at 14 V and 0.44 cd A⁻¹, respectively. The device fabricated with C1 emitter also exhibited a comparable performance with $\eta_{L,max}$ of 0.44 cd A⁻¹ and L_{max} of 726 cd m⁻² at 16 V.

The group of red polymer OLEDs made with **C2** and **C3** molecules showed similar electroluminescence spectra with maximum emission at 680 nm but with worse work parameters. Maximum current efficiency ($\eta_{L,max}$) and maximum brightness (L_{max}) were found to be 0.19 cd A^{-1} and 255 cd m^{-2} at 17 V for the **C2** device; $\eta_{L,max}$ and L_{max} were -0.055 cd A^{-1} and 146 cd m^{-2} at 16 V for device **C3**. The implementation of **C4** molecules as the emitter in polymer OLEDs allowed us to achieve near-infrared EL emission with a maximum at 765 nm. However, poor performance parameters, such as an L_{max} of 20 cd m^{-2} at 22V and an $\eta_{L,max}$ less than 0.002 cd A^{-1} were obtained. Such extremely low efficiency can be partially explained that emission of the device is on the edge of visible spectra and sensitivity of photometric equipment used in this work.

To sum up, a series of solution-processed, three layer OLEDs have been fabricated, where green polymer exciplex PVK:PO-T2T was incorporated as a host, and studied materials as the emitters. It was shown that, in the series of donor-acceptor D- π -A- π -D emitters, different acceptors had influence not only on photoluminescence but also on electroluminescence properties. This allowed the shift of EL spectra of OLEDs from green to near-infrared color. Studied OLEDs displayed extremely low current efficiency; for that reason external quantum efficiency and power efficiency of devices were not discussed. The low photoluminescence quantum yield, strong concentration quenching in the solid state and fluorescence nature of emitters may be responsible for the limited the efficiency of fabricated polymer OLEDs.

4. Conclusions

The series of new D- π -A- π -D compounds were synthesized, and their optical, photophysical, and electrochemical properties were studied. It was found that introducing different acceptor moieties in studied D- π -A- π -D compounds allows a narrow optical bandgap, and the consequential shift fluorescence emission from the green to near-infrared part of spectra. Moreover, D- π -A- π -D materials displayed a positive solvatochromic effect, which suggests charge transfer character of the emissive states. Besides that, electrochemical measurements revealed that the acceptor units significantly changed not only the reduction potential related to the LUMO, but also the oxidation potential related to the HOMO. The oxidation onset depended on choice of acceptor, and ranged from -0.12 V for **C4** up to 0.4 V for **C1**. 2,1,3-Benzoselenadiazole was identified as an acceptor unit which modified both the LUMO and HOMO energy levels and led to compounds with narrow energy gaps. Finally, the studied materials were implemented in prototype OLEDs as the emitters, together with green polymer exciplex PVK:PO-T2T as a host. The maximum EL intensities of solution-processable polymer devices based on **C5**, **C1**, **C2**, **C3**, and **C4** emitters were observed at 565 nm, 602 nm, 680 nm, 680 nm, and 765 nm, respectively.

Supplementary Materials: The following are available online at <http://www.mdpi.com/2079-4991/9/8/1179/s1>: Figures S1–S15: ^{13}C -NMR and ^1H -NMR spectra. Figure S16. UV-Vis and photoluminescence spectra of studied compounds, measured in different solvents. Figure S17. Photoluminescence spectra of emitters in the different solvents, 1 wt% in zeonex matrix and in pristine films. Figure S18. Photoluminescence decay curves of studied compounds in the different solutions (10^{-5} M in toluene, chloroform, THF, DCM) at the maximum emission. Figure S19. Normalized absorption spectra of the emitters in toluene solution and PL spectrum of PVK:PO-T2T in film. Figure S20. Normalized photoluminescence spectra of thin layers: PVK:PO-T2T doped with 1, 2, 5, 8, 10 wt% of studied molecules.

Author Contributions: Conceptualization, P.L.; data curation, P.L., M.C., and R.M.; formal analysis, P.L., G.W.-S., M.C., and R.M.; Funding acquisition, P.L.; investigation, P.L., M.C., and R.M.; methodology, P.L., and G.W.-S.; project administration, P.L.; resources, P.L.; supervision, P.L. and G.W.-S.; validation, P.L. and G.W.-S.; visualization, P.L., M.C., and R.M.; writing—original draft, P.L., M.C., and R.M.; writing—reviewing and editing, P.L., M.C., and G.W.-S.

Funding: This research was financed by budgetary funds for science in 2016–2019, under grant no. 0440/IP3/2016/74, project Iuventus Plus, Poland. M.C. and G.W.-S. are grateful for the financial support of grants 674990 EXCILIGHTH2020-MSCA-ITN-2015 and TANGO2/340019/NCBR/2017-NCBR.

Conflicts of Interest: The authors declare no conflict of interest.

References

1. Cheng, N.; Zhang, C.; Liu, Y. Tuning the electronic and optical properties of NDT-based conjugated polymers by adopting fused heterocycles as acceptor units: A theoretical study. *J. Mol. Model.* **2017**, *23*, 225. [[CrossRef](#)] [[PubMed](#)]
2. Pandey, L.; Risko, C.; Norton, J.E.; Brédas, J.L. Donor Acceptor Copolymers of Relevance for Organic Photovoltaics: A Theoretical Investigation of the Impact of Chemical Structure Modifications on the Electronic and Optical Properties. *Macromolecules* **2012**, *45*, 6405–6414. [[CrossRef](#)]
3. Zaugg, K.; Velasco, J.; Robins, K.A.; Lee, D.C. Understanding the Electronic Properties of Acceptor–Acceptor–Acceptor Triads. *ACS Omega* **2019**, *4*, 5434–5441. [[CrossRef](#)]
4. Mancilha, F.S.; DaSilveira Neto, B.A.; Lopes, A.S.; Moreira, P.F.; Quina, F.H.; Gonçalves, R.S.; Dupont, J. Are molecular 5,8-pi-extended quinoxaline derivatives good chromophores for photoluminescence applications? *Eur. J. Org. Chem.* **2006**, *2006*, 4924–4933. [[CrossRef](#)]
5. Ata, I.; Popovic, D.; Lindén, M.; Mishra, A.; Bäuerle, P. The influence of the central acceptor unit on the optoelectronic properties and photovoltaic performance of A–D–A–D–A-type co-oligomers. *Org. Chem. Front.* **2017**, *4*, 755–766. [[CrossRef](#)]
6. Wood, S.; Kim, J.H.; Wade, J.; Park, J.B.; Hwang, D.H.; Kim, J.S. Systematic control of heteroatoms in donor–acceptor copolymers and its effects on molecular conformation and photovoltaic performance. *J. Mater. Chem. C* **2016**, *4*, 7966–7978. [[CrossRef](#)]
7. Blouin, N.; Michaud, A.; Gendron, D.; Wakim, S.; Blair, E.; Neagu-Plesu, R.; Belletête, M.; Durocher, G.; Tao, Y.; Leclerc, M. Toward a Rational Design of Poly(2,7-Carbazole) Derivatives for Solar Cells. *J. Am. Chem. Soc.* **2008**, *130*, 732–742. [[CrossRef](#)] [[PubMed](#)]
8. Graf, A.; Murawski, C.; Zakharko, Y.; Zaumseil, J.; Gather, M.C. Infrared Organic Light-Emitting Diodes with Carbon Nanotube Emitters. *Adv. Mater.* **2018**, *30*, 1706711. [[CrossRef](#)]
9. Qin, W.; Ding, D.; Liu, J.; Yuan, W.Z.; Hu, Y.; Liu, B.; Tang, B.Z. Biocompatible Nanoparticles with Aggregation-Induced Emission Characteristics as Far-Red/Near-Infrared Fluorescent Bioprobes for In Vitro and In Vivo Imaging Applications. *Adv. Funct. Mater.* **2012**, *22*, 771–779. [[CrossRef](#)]
10. Kim, D.H.; D’Aléo, A.; Chen, X.K.; Sandanayaka, A.D.S.; Yao, D.; Zhao, L.; Komino, T.; Zaborova, E.; Canard, G.; Tsuchiya, Y.; et al. High-efficiency electroluminescence and amplified spontaneous emission from a thermally activated delayed fluorescent near-infrared emitter. *Nat. Photonics* **2018**, *12*, 98–104. [[CrossRef](#)]
11. Luo, D.; Chen, Q.; Qiu, Y.; Zhang, M.; Liu, B. Device Engineering for All-Inorganic Perovskite Light-Emitting Diodes. *Nanomaterials* **2019**, *9*, 1007. [[CrossRef](#)]
12. Fu, H.; Cheng, Y.M.; Chou, P.T.; Chi, Y. Feeling blue? Blue phosphors for OLEDs. *Mater. Today* **2011**, *14*, 472–479. [[CrossRef](#)]
13. Li, J.; Yan, J.; Wen, D.; Khan, W.U.; Shi, J.; Wu, M.; Su, Q.; Tanner, P.A. Advanced red phosphors for white light-emitting diodes. *J. Mater. Chem. C* **2016**, *4*, 8611–8623. [[CrossRef](#)]
14. Yersin, H. *Highly Efficient OLEDs with Phosphorescent Materials*; Wiley-VCH: Weinheim, Germany, 2007.
15. Uoyama, H.; Goushi, K.; Shizu, K.; Nomura, H.; Adachi, C. Highly efficient organic light-emitting diodes from delayed fluorescence. *Nature* **2012**, *492*, 234–238. [[CrossRef](#)]
16. Tao, Y.; Yuan, K.; Chen, T.; Xu, P.; Li, H.; Chen, R.; Zheng, C.; Zhang, L.; Huang, W. Thermally Activated Delayed Fluorescence Materials Towards the Breakthrough of Organoelectronics. *Adv. Mater.* **2014**, *26*, 7931–7958. [[CrossRef](#)]
17. Zeng, W.; Lai, H.Y.; Lee, W.K.; Jiao, M.; Shiu, Y.J.; Zhong, C.; Gong, S.; Zhou, T.; Xie, G.; Sarma, M.; et al. Achieving Nearly 30% External Quantum Efficiency for Orange-Red Organic Light Emitting Diodes by Employing Thermally Activated Delayed Fluorescence Emitters Composed of 1,8-Naphthalimide–Acridine Hybrids. *Adv. Mater.* **2018**, *30*, 1704961. [[CrossRef](#)]
18. Godumala, M.; Choi, S.; Cho, M.J.; Choi, D.H. Recent breakthroughs in thermally activated delayed fluorescence organic light emitting diodes containing non-doped emitting layers. *J. Mater. Chem. C* **2019**, *7*, 2172–2198. [[CrossRef](#)]
19. Jeon, S.K.; Park, H.J.; Lee, J.Y. Highly Efficient Soluble Blue Delayed Fluorescent and Hyperfluorescent Organic Light-Emitting Diodes by Host Engineering. *ACS Appl. Mater. Interfaces* **2018**, *10*, 5700–5705. [[CrossRef](#)]

20. Nakanotani, H.; Higuchi, T.; Furukawa, T.; Masui, K.; Morimoto, K.; Numata, M.; Tanaka, H.; Sagara, Y.; Yasuda, T.; Adachi, C. High-efficiency organic light-emitting diodes with fluorescent emitters. *Nat. Commun.* **2014**, *5*, 4016. [[CrossRef](#)]
21. Yamanaka, T.; Nakanotani, H.; Hara, S.; Hirohata, T.; Adachi, C. Near-infrared organic light-emitting diodes for biosensing with high operating stability. *Appl. Phys. Express* **2017**, *10*, 074101. [[CrossRef](#)]
22. Wang, S.; Yan, X.; Cheng, Z.; Zhang, H.; Liu, Y.; Wang, Y. Highly Efficient Near-Infrared Delayed Fluorescence Organic Light Emitting Diodes Using a Phenanthrene-Based Charge-Transfer Compound. *Angew. Chem. Int. Ed.* **2015**, *54*, 13068–13072. [[CrossRef](#)]
23. Wang, C.; Li, X.L.; Gao, Y.; Wang, L.; Zhang, S.; Zhao, L.; Lu, P.; Yang, B.; Su, S.J.; Ma, Y. Efficient Near-Infrared (NIR) Organic Light-Emitting Diodes Based on Donor-Acceptor Architecture: An Improved Emissive State from Mixing to Hybridization. *Adv. Opt. Mater.* **2017**, *5*, 1700441. [[CrossRef](#)]
24. Li, C.; Duan, R.; Liang, B.; Han, G.; Wang, S.; Ye, K.; Liu, Y.; Yi, Y.; Wang, Y. Deep-Red to Near-Infrared Thermally Activated Delayed Fluorescence in Organic Solid Films and Electroluminescent Devices. *Angew. Chem. Int. Ed.* **2017**, *56*, 11525–11529. [[CrossRef](#)]
25. Zampetti, A.; Minotto, A.; Squeo, B.M.; Gregoriou, V.G.; Allard, S.; Scherf, U.; Chochos, C.L.; Cacialli, F. Highly Efficient Solid-State Near-infrared Organic Light-Emitting Diodes incorporating A-D-A Dyes based on α,β -unsubstituted “BODIPY” Moieties. *Sci. Rep.* **2017**, *7*, 1611. [[CrossRef](#)]
26. Zampetti, A.; Minotto, A.; Cacialli, F. Near-Infrared (NIR) Organic Light-Emitting Diodes (OLEDs): Challenges and Opportunities. *Adv. Funct. Mater.* **2019**, 1807623. [[CrossRef](#)]
27. Wex, B.; Kaafarani, B.R. Perspective on carbazole-based organic compounds as emitters and hosts in TADF applications. *J. Mater. Chem. C* **2017**, *5*, 8622–8653. [[CrossRef](#)]
28. Xu, J.; Ji, Q.; Kong, L.; Du, H.; Ju, X.; Zhao, J. Soluble Electrochromic Polymers Incorporating Benzosenadiazole and Electron Donor Units (Carbazole or Fluorene): Synthesis and Electronic-Optical Properties. *Polymers* **2018**, *10*, 450. [[CrossRef](#)]
29. Ledwon, P.; Thomson, N.; Angioni, E.; Findlay, N.J.; Skabara, P.J.; Domagala, W. The role of structural and electronic factors in shaping the ambipolar properties of donor–acceptor polymers of thiophene and benzothiadiazole. *RSC Adv.* **2015**, *5*, 77303–77315. [[CrossRef](#)]
30. Yin, X.; Sun, H.; Zeng, W.; Xiang, Y.; Zhou, T.; Ma, D.; Yang, C. Manipulating the LUMO distribution of quinoxaline-containing architectures to design electron transport materials: Efficient blue phosphorescent organic light-emitting diodes. *Org. Electron.* **2016**, *37*, 439–447. [[CrossRef](#)]
31. Liu, X.; He, R.; Shen, W.; Li, M. Molecular design of donor–acceptor conjugated copolymers based on C, Si and N-bridged dithiophene and thienopyrroledione derivatives units for organic solar cells. *J. Power Sources* **2014**, *245*, 217–223. [[CrossRef](#)]
32. Takimiya, K.; Osaka, I.; Nakano, M. π -Building Blocks for Organic Electronics: Reevaluation of “Inductive” and “Resonance” Effects of π -Electron Deficient Units. *Chem. Mater.* **2014**, *26*, 587–593. [[CrossRef](#)]
33. Sandanayaka, A.S.D.; Matsushima, T.; Adachi, C. Degradation Mechanisms of Organic Light-Emitting Diodes Based on Thermally Activated Delayed Fluorescence Molecules. *J. Phys. Chem. C* **2015**, *119*, 23845–23851. [[CrossRef](#)]
34. Wong, M.Y.; Zysman-Colman, E. Purely Organic Thermally Activated Delayed Fluorescence Materials for Organic Light-Emitting Diodes. *Adv. Mater.* **2017**, *29*, 1605444. [[CrossRef](#)]
35. Sun, K.; Chu, D.; Cui, Y.; Tian, W.; Sun, Y.; Jiang, W. Near-infrared thermally activated delayed fluorescent dendrimers for the efficient non-doped solution-processed organic light-emitting diodes. *Org. Electron.* **2017**, *48*, 389–396. [[CrossRef](#)]
36. Radosław, M.; Sebastian, S.; Suwiński Jerzy, W. Simple synthesis of non-symmetric 1,4-dialkoxybenzenes via 4-alkoxyphenols. *Org. Commun.* **2016**, *9*, 23–31.
37. Shi, J.; Huang, M.; Xin, Y.; Chen, Z.; Gong, Q.; Xu, S.; Cao, S. Synthesis and characterization of a series of carbazole-based monolithic photorefractive molecules. *Mater. Lett.* **2005**, *59*, 2199–2203. [[CrossRef](#)]
38. Yang, Z.; Zhao, N.; Sun, Y.; Miao, F.; Liu, Y.; Liu, X.; Zhang, Y.; Ai, W.; Song, G.; Shen, X.; et al. Highly selective red and green-emitting two-photon fluorescent probes for cysteine detection and their bio-imaging in living cells. *Chem. Commun.* **2012**, *48*, 3442. [[CrossRef](#)]

39. Barpuzary, D.; Patra, A.S.; Vaghasiya, J.V.; Solanki, B.G.; Soni, S.S.; Qureshi, M. Highly Efficient One-Dimensional ZnO Nanowire-Based Dye-Sensitized Solar Cell Using a Metal-Free, D- π -A-Type, Carbazole Derivative with More than 5% Power Conversion. *ACS Appl. Mater. Interfaces* **2014**, *6*, 12629–12639. [[CrossRef](#)]
40. Ledwon, P.; Zassowski, P.; Jarosz, T.; Lapkowski, M.; Wagner, P.; Cherpak, V.; Stakhira, P. A novel donor-acceptor carbazole and benzothiadiazole material for deep red and infrared emitting applications. *J. Mater. Chem. C* **2016**, *4*, 2219–2227. [[CrossRef](#)]
41. Mee, S.P.H.; Lee, V.; Baldwin, J.E. Significant Enhancement of the Stille Reaction with a New Combination of Reagents—Copper(I) Iodide with Cesium Fluoride. *Chem. Eur. J.* **2005**, *11*, 3294–3308. [[CrossRef](#)]
42. Branowska, D.; Olender, E.; Wysocki, W.; Karczmarzyk, Z.; Bancierz, I.; Ledwon, P.; Lapkowski, M.; Mirosław, B.; Urbańczyk-Lipkowska, Z.; Kalicki, P. Synthesis and electrochemical characterization of oligothiophenes with 1,2,4-triazine and 5,5'-bi-1,2,4-triazine as strong electron acceptor units. *Electrochim. Acta* **2016**, *214*, 19–30. [[CrossRef](#)]
43. Drewniak, A.; Tomczyk, M.; Hanusek, L.; Mielanczyk, A.; Walczak, K.; Nitschke, P.; Hajduk, B.; Ledwon, P. The Effect of Aromatic Diimide Side Groups on the π -Conjugated Polymer Properties. *Polymers* **2018**, *10*, 487. [[CrossRef](#)]
44. Djurovich, P.I.; Mayo, E.I.; Forrest, S.R.; Thompson, M.E. Measurement of the lowest unoccupied molecular orbital energies of molecular organic semiconductors. *Org. Electron.* **2009**, *10*, 515–520. [[CrossRef](#)]
45. Cardona, C.M.; Li, W.; Kaifer, A.E.; Stockdale, D.; Bazan, G.C. Electrochemical considerations for determining absolute frontier orbital energy levels of conjugated polymers for solar cell applications. *Adv. Mater.* **2011**, *23*, 2367–2371. [[CrossRef](#)]
46. Pluczyk, S.; Vasylieva, M.; Data, P. Using Cyclic Voltammetry, UV-Vis-NIR, and EPR Spectroelectrochemistry to Analyze Organic Compounds. *J. Vis. Exp.* **2018**, *140*, e56656. [[CrossRef](#)]
47. Liu, X.; Sun, Y.; Hsu, B.B.Y.; Lorbach, A.; Qi, L.; Heeger, A.J.; Bazan, G.C. Design and Properties of Intermediate-Sized Narrow Band-Gap Conjugated Molecules Relevant to Solution-Processed Organic Solar Cells. *J. Am. Chem. Soc.* **2014**, *136*, 5697–5708. [[CrossRef](#)]
48. Zhu, H.; Huang, W.; Huang, Y.; Yang, J.; Wang, W. Narrow band-gap donor-acceptor copolymers based on diketopyrrolopyrrole and diphenylethene: Synthesis, characterization and application in field effect transistor. *Dyes Pigments* **2016**, *127*, 37–44. [[CrossRef](#)]
49. Bian, L.; Zhu, E.; Tang, J.; Tang, W.; Zhang, F. Recent progress in the design of narrow bandgap conjugated polymers for high-efficiency organic solar cells. *Prog. Polym. Sci.* **2012**, *37*, 1292–1331. [[CrossRef](#)]
50. Cao, X.; Tong, J.; He, Z.; Zhang, M.; Zhang, X.; Ma, J.; Gao, P.; Li, J.; Zhang, P.; Wang, C.; et al. An extremely narrow band gap conjugated polymer for photovoltaic devices covering UV to near-infrared light. *Dyes Pigments* **2018**, *158*, 319–325. [[CrossRef](#)]
51. İcli-Özkut, M.; İpek, H.; Karabay, B.; Cihaner, A.; Önal, A.M. Furan and benzochalcogenodiazole based multichromic polymers via a donor acceptor approach. *Polym. Chem.* **2013**, *4*, 2457. [[CrossRef](#)]
52. Regis, E.; de Aguiar, L.O.; Tuzimoto, P.; Girotto, E.; Frizon, T.E.; Dal Bó, A.G.; Zapp, E.; Marra, R.; Gallardo, H.; Vieira, A.A. Effect of heteroatom exchange (S/Se) in the mesomorphism and physical properties of benzochalcogenodiazole-based liquid crystals. *Dyes Pigments* **2018**, *157*, 109–116. [[CrossRef](#)]
53. Aguiar, L.; Regis, E.; Tuzimoto, P.; Girotto, E.; Bechtold, I.H.; Gallardo, H.; Vieira, A.A. Investigation of thermal and luminescent properties in 4,7-diphenylethynyl-2,1,3-benzothiadiazole systems. *Liq. Cryst.* **2018**, *45*, 49–58. [[CrossRef](#)]
54. Kayi, H.; Elkamel, A. A theoretical investigation of 4,7-di(furan-2-yl)benzo[c][1,2,5]selenadiazole-based donor-acceptor type conjugated polymer. *Comput. Theor. Chem.* **2015**, *1054*, 38–45. [[CrossRef](#)]
55. Li, H.; Guo, Y.; Lei, Y.; Gao, W.; Liu, M.; Chen, J.; Hu, Y.; Huang, X.; Wu, H. D- π -A benzo[c][1,2,5]selenadiazole-based derivatives via an ethynyl bridge: Photophysical properties, solvatochromism and applications as fluorescent sensors. *Dyes Pigments* **2015**, *112*, 105–115. [[CrossRef](#)]
56. Karabay, L.C.; Karabay, B.; Karakoy, M.S.; Cihaner, A. Effect of furan, thiophene and selenophene donor groups on benzoselenadiazole based donor-acceptor-donor systems. *J. Electroanal. Chem.* **2016**, *780*, 84–89. [[CrossRef](#)]
57. Simokaitiene, J.; Grazulevicius, J.V.; Jankauskas, V.; Rutkaite, R.; Sidaravicius, J. Synthesis and properties of glass-forming phenothiazine and carbazole adducts. *Dyes Pigments* **2008**, *79*, 40–47. [[CrossRef](#)]

58. Kirkus, M.; Simokaitiene, J.; Grazulevicius, J.V.; Jankauskas, V. Phenyl, carbazolyl and fluorenyl-substituted derivatives of indolo[3,2-b]carbazole as hole-transporting glass forming materials. *Synth. Met.* **2010**, *160*, 750–755. [[CrossRef](#)]
59. Chosrovian, H.; Rentsch, S.; Grebner, D.; Dahm, D.U.; Birckner, E.; Naarmann, H. Time-resolved fluorescence studies on thiophene oligomers in solution. *Synth. Met.* **1993**, *60*, 23–26. [[CrossRef](#)]
60. Tsami, A.; Bünnagel, T.W.; Farrell, T.; Scharber, M.; Choulis, S.A.; Brabec, C.J.; Scherf, U. Alternating quinoxaline/oligothiophene copolymers—Synthesis and unexpected absorption properties. *J. Mater. Chem.* **2007**, *17*, 1353–1355. [[CrossRef](#)]
61. Sanzone, A.; Calascibetta, A.; Ghiglietti, E.; Ceriani, C.; Mattioli, G.; Mattiello, S.; Sassi, M.; Beverina, L. Suzuki–Miyaura Micellar One-Pot Synthesis of Symmetrical and Unsymmetrical 4,7-Diaryl-5,6-difluoro-2,1,3-benzothiadiazole Luminescent Derivatives in Water and under Air. *J. Org. Chem.* **2018**, *83*, 15029–15042. [[CrossRef](#)]
62. Jheng, J.F.; Lai, Y.Y.; Wu, J.S.; Chao, Y.H.; Wang, C.L.; Hsu, C.S. Influences of the Non-Covalent Interaction Strength on Reaching High Solid-State Order and Device Performance of a Low Bandgap Polymer with Axisymmetrical Structural Units. *Adv. Mater.* **2013**, *25*, 2445–2451. [[CrossRef](#)]
63. Cihaner, A.; Algı, F. A Novel Neutral State Green Polymeric Electrochromic with Superior n and p-Doping Processes: Closer to Red-Blue-Green (RGB) Display Realization. *Adv. Funct. Mater.* **2008**, *18*, 3583–3589. [[CrossRef](#)]
64. Wang, L.; Huang, W.; Li, R.; Gehrig, D.; Blom, P.W.M.; Landfester, K.; Zhang, K.A.I. Structural Design Principle of Small-Molecule Organic Semiconductors for Metal-Free, Visible-Light-Promoted Photocatalysis. *Angew. Chem. Int. Ed.* **2016**, *55*, 9783–9787. [[CrossRef](#)]
65. Gibson, G.L.; McCormick, T.M.; Seferos, D.S. Atomistic Band Gap Engineering in Donor–Acceptor Polymers. *J. Am. Chem. Soc.* **2012**, *134*, 539–547. [[CrossRef](#)]
66. Belfield, K.D.; Ren, X.; Van Stryland, E.W.; Hagan, D.J.; Dubikovskiy, V.; Miesak, E.J. Near-IR Two-Photon Photoinitiated Polymerization Using a Fluorone/Amine Initiating System. *J. Am. Chem. Soc.* **2000**, *122*, 1217–1218. [[CrossRef](#)]
67. De Boni, L.; Fonseca, R.D.; Cardoso, K.R.A.; Grova, I.; Akcelrud, L.; Correa, D.S.; Mendonça, C.R. Characterization of two and three-photon absorption of polyfluorene derivatives. *J. Polym. Sci. Part B Polym. Phys.* **2014**, *52*, 747–754. [[CrossRef](#)]
68. Li, Y.; Li, X.L.; Chen, D.; Cai, X.; Xie, G.; He, Z.; Wu, Y.C.; Lien, A.; Cao, Y.; Su, S.J. Design Strategy of Blue and Yellow Thermally Activated Delayed Fluorescence Emitters and Their All-Fluorescence White OLEDs with External Quantum Efficiency beyond 20%. *Adv. Funct. Mater.* **2016**, *26*, 6904–6912. [[CrossRef](#)]
69. Chapran, M.; Lytvyn, R.; Begel, C.; Wiosna-Salyga, G.; Ulanski, J.; Vasylieva, M.; Volyniuk, D.; Data, P.; Grazulevicius, J.V. High-triplet-level phthalimide based acceptors for exciplexes with multicolor emission. *Dyes Pigments* **2019**, *162*, 872–882. [[CrossRef](#)]
70. Pander, P.; Gogoc, S.; Colella, M.; Data, P.; Dias, F.B. Thermally Activated Delayed Fluorescence in Polymer–Small-Molecule Exciplex Blends for Solution-Processed Organic Light-Emitting Diodes. *ACS Appl. Mater. Interfaces* **2018**, *10*, 28796–28802. [[CrossRef](#)]
71. Porcu, P.; Vonlanthen, M.; González-Méndez, I.; Ruiu, A.; Rivera, E. Design of Novel Pyrene-Bodipy Dyads: Synthesis, Characterization, Optical Properties, and FRET Studies. *Molecules* **2018**, *23*, 2289. [[CrossRef](#)]

